PERGAMON

Journal of Structural Geology 25 (2003) 1575–1585

JOURNAL OF STRUCTURAL GEOLOGY

www.elsevier.com/locate/jsg

On the rheology of partially molten synthetic granite

J. Mecklenburgh*, E.H. Rutter

Rock Deformation Laboratory, Department of Earth Sciences, University of Manchester, Manchester M13 9PL, UK

Received 21 May 2002; received in revised form 11 December 2002; accepted 5 January 2003

Abstract

In an attempt to obviate some of the difficulties inherent in using natural rocks to study experimentally the rheology of partially-molten granitic rocks, we report some preliminary experiments using hot-pressed synthetic aggregates, with quartz as the solid phase and a quartz–albite glass to form the melt phase. Undrained constant displacement rate and stress relaxation experiments were performed at 1100 °C and 300 MPa total confining pressure using nominally 16 and 28 wt% anhydrous melt, and at 980 °C with 12 wt% of water-saturated melt. Strain rate varies non-linearly with stress, corresponding to a stress exponent of 3.6 for the anhydrous melt tests, and 1.9 with the wet melt. Strain rate is enhanced about 160-fold through doubling the melt fraction from 16 wt%. Intracrystalline plasticity appears to contribute insignificantly to the observed deformation, and the preservation of relatively equant grains implies a granular flow process. Microcracking occurs during isostatic hot-pressing, and also contributes to subsequent non-isostatic deformation at high stresses and strain rates. Models of flow of partially molten rock that assume diffusive transfer accommodation of granular flow predict linear viscosity but only at lower strain rates than accessed experimentally. It is suggested that the non-linear granular flow observed in these experiments involved the episodic unsticking of sintered contacts between grains by a rate-dependent cracking and/or dislocation accommodation process.

Keywords: Granite; Partially molten; Rheology

1. Introduction

The presence of substantial migmatite terrains exposed in ancient orogenic belts tells us that parts of the continental crust have been partially molten during orogenesis or during post-orogenic mafic underplating. Contemporary deep seismic reflection profiles sometimes show low velocity zones or bright reflectors that may correspond to zones of partially molten rock. For example, in central Asia it is inferred that a significant thickness of the continental crust below the Tibetan plateau is presently partially molten (Nelson et al., 1996). The large volume fraction of syn- and post-kinematic granites in the cores of many orogenic belts often implies that 40% or more of the lower crust may have been partially molten at some stage.

The rheological behaviour of partially molten crustal rocks is important from two points of view. First, the rheological characteristics determine the kinetics of the extraction and collection of crustal melts, ultimately to ascend and be emplaced as intermediate and high-level granitic plutons. Second, partially molten rocks are expected to be exceptionally weak, and hence radically to affect the overall 'strength' of an orogen once a partially molten horizon has developed, perhaps facilitating effective mechanical decoupling of the crustal and mantle parts of the lithosphere.

The effect of partially molten rocks on the bulk rheology of the lower-middle continental crust is poorly understood. This is partly due to the relatively few experimental studies on the rheology of partially molten crustal rocks (Arzi, 1978; van der Molen and Paterson, 1979; Paquet and Francois, 1980; Paquet et al., 1981; Dell'Angelo et al., 1987; Dell'Angelo and Tullis, 1988; Rutter and Neumann, 1995; Gleason et al., 1999) and to the relative difficulty of carrying out such studies so that geologically meaningful results can be obtained. In previous experimental studies deformation of the matrix of solid grains has been observed to be accommodated by either cataclastic/frictional deformation (e.g. van der Molen and Paterson, 1979; Dell'Angelo and Tullis,

* Corresponding author. Now at and correspondence address: Bayerisches Geoinstitut, Universität Bayreuth, Bayreuth, D95440, Germany. Tel. +49-(0)921-553735; fax: +49-(0)921-553769.

E-mail address: Julian.Mecklenburgh@uni-bayreuth.de (J. Mecklenburgh).

0191-8141/03/$ - see front matter © 2003 Elsevier Science Ltd. All rights reserved.
doi:10.1016/S0191-8141(03)00014-2

1988; Rutter and Neumann, 1995) or by intracrystalline plasticity (e.g. Dell'Angelo and Tullis, 1988; Gleason et al., 1999). Although both of these processes are seen to be important in the natural deformation of some partially molten rocks, it has been speculated that at slower, natural strain rates some kind of granular flow process involving whole grains might dominate, with sliding accommodated by diffusive mass transfer processes accelerated by the presence of the melt phase (Dell'Angelo et al., 1987; Rutter and Neumann, 1995). Dell'Angelo et al. (1987) argued that this process was the dominant deformation mechanism in their experiments on fine-grained material. With granular flow or grain boundary sliding the mechanism for strain accumulation is the relative movement of grains and therefore a rock that has deformed by granular flow or grain boundary sliding could at the microscale show no evidence of having been deformed and might look like a statically crystallised rock. This might explain the apparent lack of natural examples of partially molten rocks that have deformed by granular flow. However, Sawyer (2001) observed alignment of euhedral plagioclase grains in a metapelite that underwent anatexis during contact metamorphism, and attributed this to *flow in the magmatic state* due to relatively high melt contents ~25%. On the other hand, Rosenberg and Riller (2000) show an example (from the thermal aureole of the Sudbury Igneous Complex) of granitic rocks in which quartz grains were deforming by intracrystalline plasticity whilst the rock was partially molten as a result of contact metamorphism.

Recently Rutter (1997) and Paterson (2001) have proposed simple constitutive models to describe the flow of partially molten rocks based on the concept of diffusion-accommodated granular flow. These models predict a linear-viscous rheology. In all previous experimental studies in which stress versus strain rate information was obtained, a strongly non-linear rheology was observed, which is to be expected if deformation rate is controlled either by fracture or intracrystalline–plastic processes. Understanding of the deformation of partially molten rocks in nature requires the design of experiments that favour flow by a specific deformation mechanism. In this paper, we describe an approach to the study of partially molten granitoid rheology aimed at simplifying the nature of the sample material and isolating particular deformation mechanisms. This involves the use of a synthetic 'granitoid', consisting of a single solid phase (quartz) and a near-eutectic quartz–albite melt phase. For simplicity, only one solid phase is used, and this also allows us to compare the rheology of our quartz plus melt samples with published data for pure quartz samples deformed under similar conditions (e.g. Hobbs et al., 1972; Luan and Paterson, 1992; Gleason and Tullis, 1995; Brodie and Rutter, 2000).

2. Experimental approach

Previous studies of the rheology of partially molten granitoids have most often used natural rocks except for Dell'Angelo et al. (1987) and Dell'Angelo and Tullis (1988) who used sintered quartz–feldspar aggregates, Gleason et al. (1999) who used hot-pressed aggregates of albite, potassium feldspar, quartz and biotite and van der Molen and Paterson (1979) who deformed one sample hot pressed from powdered granite. With all these approaches, the amount of melt produced and its viscosity, was determined both by the amount of water added and by the test temperature. Often, and especially for relatively coarse-grained protoliths, the melt fraction and composition has not reached equilibrium in the duration of the test, and melt-producing reactions have varied according to test temperature.

To understand the rheology of partially molten granitic rocks ideally we need to be able to control all of the following:

1. The test temperature, total confining pressure and (independently) the melt pressure.
2. The mineralogy of the solid phase(s) and the melt composition, and the latter ideally should not vary with test temperature.
3. The water content of the melt and the melt viscosity.
4. The grain size of the solid phase(s).
5. The melt fraction.

Unfortunately, several of these variables cannot be controlled independently. Temperature and total confining pressure can be controlled, and also potentially the melt pressure (Rutter and Neumann, 1995; Viskupic et al., 2001). However, melt pressure (and hence effective pressure) can vary during the time-scale of an experiment independently relative to confining pressure, either due to compaction or dilatation induced by elastic or permanent deformation (Renner et al., 2000). This effect depends on melt viscosity, grain size and melt connectivity. The melt viscosity is unfortunately dependent on the composition, the water content and the temperature, and hence cannot be independently controlled. The melt fraction is likely to vary with temperature, water content and time if the melt has solubility for the solid phase(s).

To attempt to obviate some of these difficulties, we have carried out preliminary experiments using a granite-like, hot-pressed aggregate of quartz grains mixed with a Na_2O–Al_2O_3–SiO_2 glass. The methodology of these experiments is the same as that used by Hirth and Kohlstedt (1995a,b) to study the rheology of partially molten ultrabasic rocks, in which olivine powder was mixed with a basaltic glass and re-fused. In principle the grain size of the solid phase, the melt fraction and its composition (except for any dissolution of silica in the melt), and the water content can be controlled. In practice it proved difficult to control the grain size of quartz grains because they tended to fracture

during initial pressurization. Also, without weld-sealing the sample within a ductile metal cylinder it is difficult in the apparatus used to prevent loss of some water (in a water-added sample) during hot-pressing, and hence to be certain of the water content of the melt during an experiment.

3. Sample preparation

3.1. The melt phase

The melt phase was prepared by mixing the required quantities of Al_2O_3, Na_2CO_3 and SiO_2 analytical reagents to obtain a composition close to the anhydrous eutectic of the quartz–albite system at 300 MPa with approximately 17 mol% excess Na_2O. Experience showed that the excess soda led to more effective and uniform fusion of the mixture to form a clear glass, compensated for some evaporation of sodium during fusion, and facilitated spreading of the melt through the aggregate and compaction during hot-pressing. Values for the eutectic melt composition were taken from Wen and Nekvasil (1994). They give, under anhydrous conditions at 300 MPa, the eutectic composition to be 0.249 mole fraction quartz. The eutectic temperature under these conditions is 1076 °C. The following equation shows the molar proportions of oxides used and the resulting glass composition:

$$0.588Na_2CO_3 + 0.3755Al_2O_3 + 2.502SiO_2 \rightarrow 0.249SiO_2 + 0.751NaAlSi_3O_8 + 0.213Na_2O + 0.588CO_2\uparrow$$

The oxide powders were stirred in a tumbler bottle with zirconia balls for 1 h to produce even mixing. This mixture was placed in a furnace and heated 1100 °C in air in an aluminium oxide crucible for 12 h to produce decarbonation and eventually a clear glass. Thin sections of the glass were made to confirm that all the components had melted. The glass was then crushed to a fine powder in a tungsten carbide mortar. ICP-AES analysis of the glass annealed for 12 h at 1100 °C and 300 MPa showed that it had the composition 37.4 mol% quartz, 45.7 mol% albite, 16.9 mol% excess Na_2O (corresponding to 69 wt% SiO_2, 16 wt% Na_2O and 15 wt% Al_2O_3).

3.2. The solid phase

A natural quartz beach sand, sieved to separate the range 63–120 μm, was used as the solid phase. The grain size was chosen as a compromise between maximising permeability of the aggregate whilst minimising the tendency for impingement cracking during hot pressing and densification of the mixture. The sand was heated for 12 h at 900 °C in a one-atmosphere furnace to dry the surfaces and hopefully to decrepitate any water inclusions that might exist in some grains.

3.3. Hot pressing

The quartz and glass powders were mixed in appropriate proportions in order to give the desired melt fraction. The mixture was initially uniaxially cold-pressed at 150 MPa in a 0.2 mm wall thickness iron tube to eliminate some of the porosity but without inducing extensive impingement cracking of the quartz grains. The resulting 25 mm long and 9.5 mm diameter sample was then hot-pressed for 12 h at the desired test temperature and 300 MPa inside an additional 0.3 mm wall thickness iron jacket, immediately after which the deformation experiment was performed. All experiments were performed using a Paterson-ANUtech, internally-heated, argon gas confining-medium testing machine (Paterson, 1990).

The above procedure resulted in samples at the beginning of the deformation experiment that were ca. 99% fully dense (Fig. 1). However, the existence of void spaces in the sample at the beginning of hot-pressing meant that there was a tendency for impingement cracking of the quartz grains to occur. To minimise this the confining pressure was slowly ramped up from an initial 150 MPa during progressive heating. Owing to the requirement to run experiments with at least 40 °C overstep with respect to the albite–quartz eutectic temperature, and the fact that the glass was peralkaline, some quartz dissolved in the melt during hot pressing, typically increasing the melt fraction by more than twice relative to the amount of glass initially added (Table 1). This promoted full densification, but caused the melt to become more silicic, and hence more viscous.

The silica and alumina content of the melt and the melt fraction was estimated after the experiment by electron microprobe. Melt fraction was measured by pixel counting on a binary image prepared by applying a threshold level to a greyscale backscattered electron image. The subjective positioning of the threshold level leads to an intrinsic uncertainty in melt fraction of about ±3%. Taking a series of 20 images along the length of a typical sample also shows variations in local mean melt fraction of about ±3%. Whereas the ratio $SiO_2/(SiO_2 + Al_2O_3)$ for the starting glass was 82 ± 1%, microprobe measurements of this ratio in melt volumes at the end of experiments averaged 87 ± 7%. This change gives some idea of the increase of silica content of the melt during deformation, that is reflected in the ±7% variability observed.

For simplicity and to establish end-member behaviour we initially used anhydrous samples with nominally 16 and 28% volume of melt after melt fraction equilibration during hot-pressing. This required testing at high temperatures (1100 °C) at which the melt viscosity is expected to be ca. 10^7 Pa s (Hess and Dingwell, 1996; Holtz et al., 1999). We also carried out some runs with ca. 1% of the total sample weight of water added, corresponding to near-saturation of the lower melt-fraction samples. This dramatically reduces the melt viscosity (by approximately 10,000-fold) at a given temperature but also reduces the eutectic temperature.

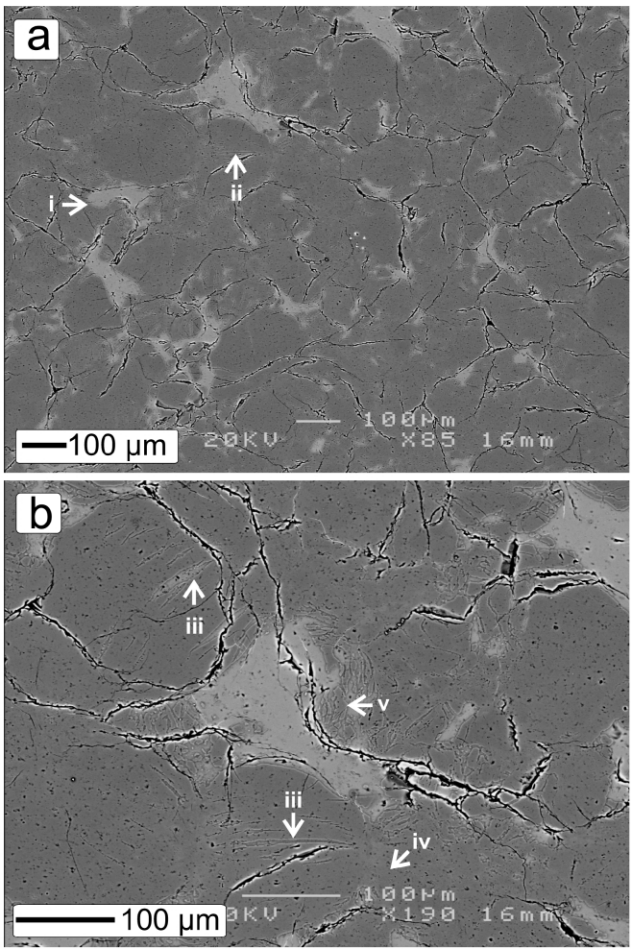

Fig. 1. Back-scattered electron images of sample SA20, hot pressed for 48 h at 1100 °C with 5 wt% glass added, giving a final melt fraction of 10 ± 4%. The melt fraction is the lighter shade of grey. Most sinuous black lines are cracks introduced during quenching and some may have developed along grain boundaries. The melt fraction is variably heterogeneously distributed, and formation of curved re-entrants (arrow i) and truncated impingement cracks (arrow ii) shows where quartz has been incorporated into the melt. In (b), early formed cracks can be seen to be filled with the melt phase (arrow iii), some quartz grain boundaries appear to be welded together (arrow iv) and there is spalling of fine fragments into the melt (v).

Addition of a measured amount of water to the glass prior to fusion but such that it is all incorporated into the glass is not straightforward in this apparatus. Because the sample jacket is pressure-sealed to the loading pistons outside the hot zone of the furnace, too rapid heating and pore collapse can result in bulging of the jacket with loss of water to the cooler ends of the loading pistons, leading to uncertainty regarding the amount of water that was actually incorporated into the melt.

4. Experiments performed

Fifteen axially-symmetric compression experiments are reported on partially molten synthetic quartz–albite rocks, at 300 MPa confining pressure and between 980 and 1160 °C (Table 1). Constant displacement rate (nominally constant strain rate), displacement-rate stepping and stress relaxation experiments were carried out. Experiments were performed nominally dry and with water added. Experiments were at pressure and temperature for different lengths of time, from 30 h up to 150 h, according to the different displacement rates used. Over the time period there was no observable increase in the melt fraction, although the uncertainty in measuring the melt fraction is large (see above). In these experiments, the melt was not allowed to escape from the sample (i.e. the samples were undrained) and therefore the pressure of the melt phase was expected to be approximately equal to the mean stress. This means that the effective confining stress will be approximately zero during the sample deformation. It was not determined whether there is any systematic effect of variations in effective pressure on the behaviour of these samples.

5. Results

The stress/strain curves (e.g. Fig. 2) were not corrected for the stress supported by the iron jacket, which is approximately 4 MPa at a strain rate of 10^{-5} s^{-1} and decreasing by about 50% per decade reduction in strain rate, and is commensurate with the uncertainty in stress measurement. Scatter in experimental results due to differences between samples is far greater than measure-

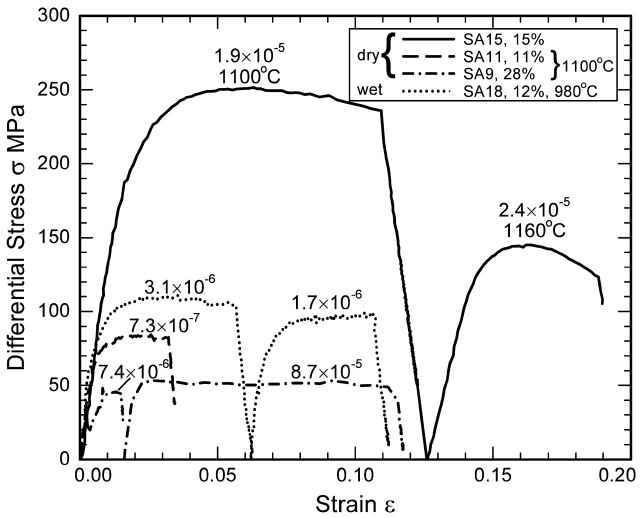

Fig. 2. Typical experimental data (undrained) at 300 MPa confining pressure and 1100 °C illustrating the effects of strain rate and melt fraction on the behaviour of dry 'synthetic' granite of 60–100 μm quartz grain size with an albite–quartz melt phase. Against each stress/strain curve the strain rate is given in s^{-1}, the melt fraction (% ± 4%) and run temperature are given in the key. The weakening effect of strain rate reduction and temperature increase at a comparable melt fraction is apparent, and of increasing the melt fraction from 15 to 28%. The apparent strain weakening seen in sample SA15 is due to the sample bending, which proved very difficult to avoid at high strains. Offloading lines link segments of strain-rate stepping tests. In run SA18 at 980 °C the melt phase was water saturated.

Table 1
Experimental details. Run conditions for the experiments reported. d-rate stepping = displacement rate stepping, T-stepping = temperature stepping, HIP = hot isostatically pressed

Test	Glass added (wt.%)	Final melt fraction (vol.%)	T (°C)	Total strain	Strain rate (s^{-1})	Flow stress (MPa)	Test type	Run duration (h)
SA9	10	28 ± 6	1100	0.12	7.4×10^{-6}	45	d-rate stepping	50.3
					8.7×10^{-5}	50		
SA11	5	11 ± 8	1100	0.03	6.8×10^{-7}	83	d-rate stepping	96
					1.2×10^{-7}	57		
SA12	5	20 ± 10	1100	0.17	7.0×10^{-6}	217	d-rate stepping	30
					3.8×10^{-5}	319		
					6.0×10^{-5}	379		
SA13	5	18 ± 6	1100	0.08	3.2×10^{-6}	140	d-rate stepping	45
					1.7×10^{-5}	173		
SA14	5	17 ± 4	1100	0.08	4.1×10^{-6}	129	d-rate stepping	78.3
SA15	5	15 ± 6	1100	0.17	1.7×10^{-5}	250	T-stepping	31.3
			1160		2.0×10^{-5}	145		
SA16	5	17 ± 6	1100	0.09	3.1×10^{-6}	135	d-rate stepping	67.8
					1.6×10^{-6}	115		
SA17	5	18 ± 6	1100	0.1	3.7×10^{-6}	100	T-stepping	32.5
			1150		3.9×10^{-6}	47		
SA18	5	14 ± 2	980	0.12	3.1×10^{-6}	107	d-rate stepping (wet melt)	150
					1.6×10^{-6}	96		
SA19	7	[a]	800	0.09	2.0×10^{-6}	200	const. d-rate (wet melt)	125
SA20	5	10 ± 4	1100				HIP	48
SA21	5	16 ± 7	1100	0.05	6.1×10^{-7}	118	d-rate stepping	42.3
					1.2×10^{-6}	112		
SA22	5	15 ± 4	1100	0.09	5.0×10^{-7}	53	const. d-rate	74.9
SA23	5	18 ± 5	1100	0.065	1.0×10^{-7}	125	const. d-rate	33

[a] Melt fraction lower than resolution of measurement because of albite crystallisation.

ment uncertainties and is on the order of ± 10% of the stress supported. This is attributed to unevenness of microstructure and variations in melt fraction from place to place within and between samples. The effect of using samples directly after individual hot-pressing in the testing machine also results in variable degrees of parallelism of the sample sides.

Some variability of temperature profile between runs is inevitable. Although during calibration, temperature variations along sample can be kept within about 3 °C, there is some deterioration of this performance with furnace ageing between calibrations.

5.1. Experiments with nominally anhydrous melt

All nominally anhydrous samples were deformed at 1100 °C and 300 MPa total confining pressure. The samples were deformed at constant displacement rates with strain rate stepping resulting in strain rates $\dot{\epsilon}$ ranging from 6×10^{-5} to 6×10^{-7} s^{-1}. In all cases, samples flowed at a constant differential stress after an initial period of elastic behaviour (Fig. 2), and after each run all samples were observed to have deformed (up to ca. 17% total strain) in a fully ductile way with no evidence of fault localization. Using this deformation apparatus, reliable rheological data cannot be gained to large sample strains because there is a tendency for the sample to kink or bend. Over this range of strain rates, samples containing 16 ± 4% melt deformed at a flow stress σ between 80 and 380 MPa (Figs. 2 and 3). The 16% melt samples were approximately four times stronger than experiments deformed with 28 ± 6% melt.

Stress relaxation tests (Rutter et al., 1978; Covey-Crump, 1992) were performed at the end of many constant displacement rate experiments to access slower strain rates than can be attained using constant displacement rate tests. Fig. 3 shows a compilation of $\log_{10}$ flow stress versus $\log_{10}$ strain rate from both constant displacement rate and stress relaxation tests. Over four orders of magnitude in strain rate, the 16% melt data show a slope of approximately $d\log\dot{\epsilon}/d\log\sigma = 3.5$. The rate of weakening with decreasing strain rate at 28% melt is approximately the same as at 16% melt.

Temperature stepping was applied in two runs (Table 1 and Fig. 2). Samples were weaker at the higher temperatures but there is presently insufficient data to draw any significant conclusions.

5.2. Experiments with water added

Samples with water added were deformed at 980 °C (SA18) and at 800 °C (SA19). Despite the lower temperature, sample SA18 showed approximately the same strength as nominally dry samples at 1100 °C in constant displacement rate tests. This is shown by the close proximity of stress relaxation data for SA18 to the constant displacement rate data at 1100 °C (Fig. 3). This may be due to the fact that

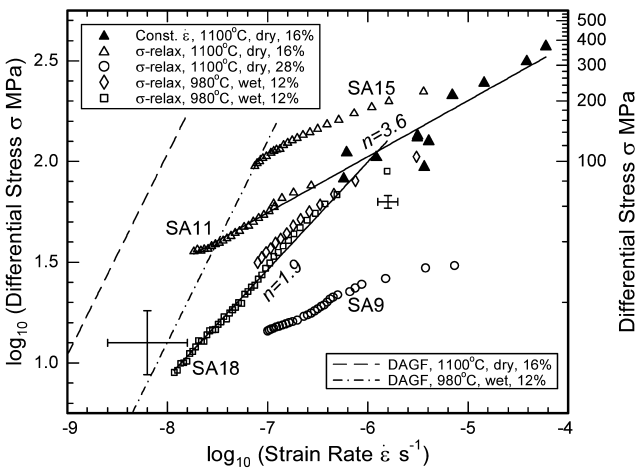

Fig. 3. Experimental data (undrained) at 300 MPa confining pressure illustrating the behaviour of 'synthetic' granite of 60–100 μm quartz grain size with an albite–quartz melt phase. 'Dry' data at 1100 °C with nominal 16 and 28% melt (constant strain rate filled triangles and stress relaxation experiments open triangles) show a fairly steady rate of reduction of strength with reducing strain rate corresponding to a stress exponent, *n*, of about 3.6. Uncertainty in the stress and strain rate for the constant strain rate data is smaller than the symbols (filled triangles). Typical uncertainties for the stress relaxation data are shown with two sets of error bars; one at low stress/strain rate and one at higher stress/strain rate. The strength at the higher melt fraction is much reduced (see stress relaxation data for SA9, open circles). For 12% melt but with the melt water-saturated and at a lower temperature, the more rapid rate of strength reduction corresponds to a stress exponent *n* of about 1.9 (open squares and diamonds). These data are compared with predictions of the theoretical model for undrained diffusion-accommodated granular flow DAGF (Rutter, 1997; stress exponent = 1) with corresponding melt fractions and a melt viscosity of 10^7 Pa s in the dry case and 10^5 Pa s in the wet case. These viscosities are estimated from the composition of the melt and the data of Holtz et al. (1999), in the wet case the melt is assumed to be water saturated (~7 wt%).

the effect of the water lowering the melt viscosity is offset to some degree by the lower temperature increasing the viscosity. On the other hand, at lower strain rates in stress relaxation tests the strength falls more rapidly with decreasing strain rate than in the dry case, corresponding to approximately $d\log\dot{\epsilon}/d\log\sigma = 1.9$. A constant displacement rate tested sample at a similar rate at 800 °C was approximately twice as strong. It was found that at these conditions albite was crystallising from the melt resulting in very low melt fractions of ca. 1%. This suggests that the sample was not saturated in water, as the wet solidus should be at approximately 700 °C.

5.3. Microstructures

For microstructural study, samples were cut in half longitudinally and the cut surfaces vacuum impregnated with epoxy resin to minimise the risk of grains plucking. Standard thin sections were prepared polished to a finish of 1 μm using Al_2O_3. SEM analysis was performed using a Jeol 6400 analytical SEM in back scattered electron (BSE) mode with an accelerating voltage of 20 kV and a probe current of 2–3 nA. In order to obtain a good contrast between the melt and the quartz grains, the sample surface had to be close to the BSE detector and also relatively high probe currents had to be used.

Perhaps surprisingly, the melt phase has a higher brightness than the quartz on the BSE images (Figs. 1 and 4). Fig. 1 shows the microstructure of an undeformed sample (SA20). It had initially 5 wt% eutectic glass added, resulting in a mean melt fraction of 0.10 ± 0.04 after being isostatically hot-pressed for 48 h. In Fig. 1 it can be seen that there are some large melt pockets (>100 μm across). The majority of grain boundaries contain melt and the sample has zero porosity. Cracks in the quartz grains contain melt within them. This implies that these cracks formed either before the sample reached a temperature above the solidus

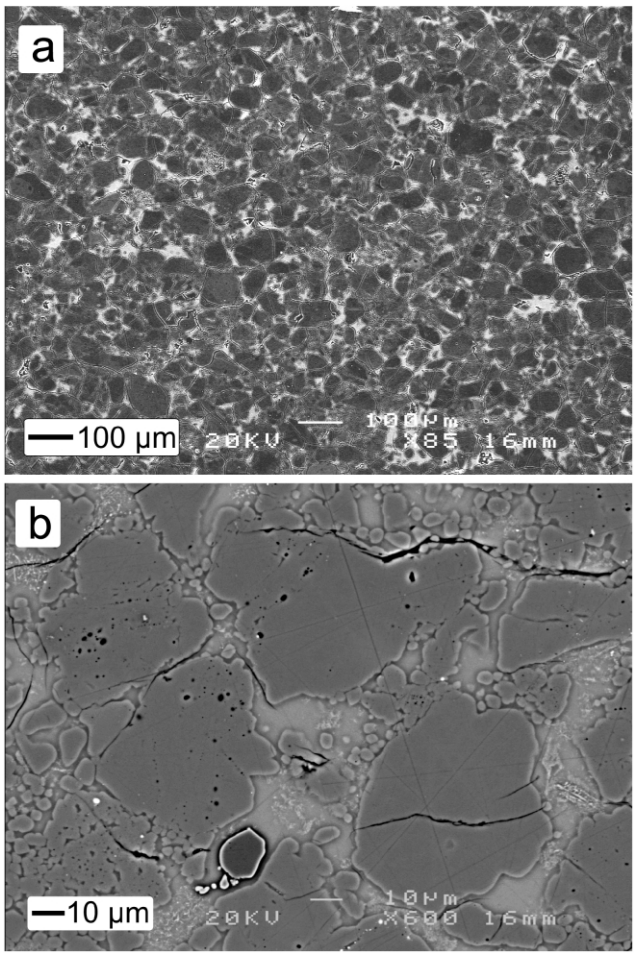

Fig. 4. Microstructures of experimentally deformed synthetic quartz/melt aggregate. (a) Sample SA11,which was axisymmetrically shortened 6% in the vertical direction at 1100 °C, dry, at a strain rate of 1 and 7×10^{-7} s^{-1}. The melt (11% volume, light grey) is fairly uniformly distributed and there is little disruptive fracturing of the grains, which remain equant. Time at temperature = 96 h. (b) Sample SA18, (18% melt, light grey) was shortened 12% in the vertical direction at 980 °C at strain rates of 3.1 and 1.6×10^{-6} s^{-1}, with the melt phase estimated to be water saturated (about 10 wt%). There is little melt-filled fracturing of the quartz grains (dark grey), zero vapour-filled porosity and growth of new, small quartz grains in the melt phase. The empty (black) cracks in the quartz are quench cracks. Time at temperature = 50 h.

or whilst the sample was at a temperature above the solidus. It is most likely that these cracks formed prior to the sample reaching the eutectic temperature due to stress intensification at grain contacts on initial pressurization.

Microstructures of deformed samples are shown in Figs. 4 and 5. Melt is evenly distributed throughout the sample and there appears to be no preferential orientation of the melt pockets. Fig. 6 shows the distribution of melt pocket long-axis orientations relative to the principal stress orientations for the image in Fig. 4a (sample SA11, deformed at relatively low differential stresses). There appears to be no preferential orientation of the melt pockets but this could be due to microstructural readjustment because the differential stress was released before the samples were quenched. One may calculate the characteristic decay time t_c it would take for the melt phase to respond to a change in melt pressure using:

$$t_c = \frac{\eta \beta_s l_c^2}{k} \quad (1)$$

where η is the melt viscosity, β_s is the storage capacity (which approximates to the melt fraction times the melt compressibility if the solid phase is assumed to be incompressible), l_c is the characteristic length scale and k is the permeability (Fischer and Paterson, 1989; Renner et al., 2000). Assuming a viscosity of 10^7 Pa s, a melt compressibility of 2×10^{-10} Pa^{-1} (after Kirschen and Pichavant, 2001), a permeability of 10^{-14} m^2 (calculated using $k = d^2\phi^3/400$ where d is the grain size and ϕ is the melt fraction) and that the characteristic length scale is of the order of the grain size 60 μm, then the time taken for the melt to flow in response to a change in stress state will be approximately 1 min. Hence it would be expected that the melt distribution would be able to readjust itself after removal of the load and before significant cooling.

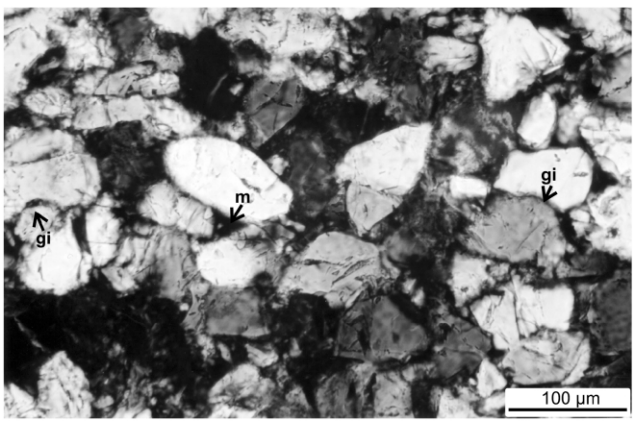

Fig. 5. Optical micrograph (crossed polars) of sample SA12 (17% strain at three different strain rates that led to high differential stresses, see Table 1). The compression direction is vertical. Melt pockets (marked by m) are often seen apparently at triple junctions between grains. Axially-oriented, melt-filled microcracks are seen in many grains and extension on these accounts for much of the apparent shape fabric. Apparent grain interpenetrations can be seen (marked by gi) which may be attributable to deformation by diffusive mass transfer.

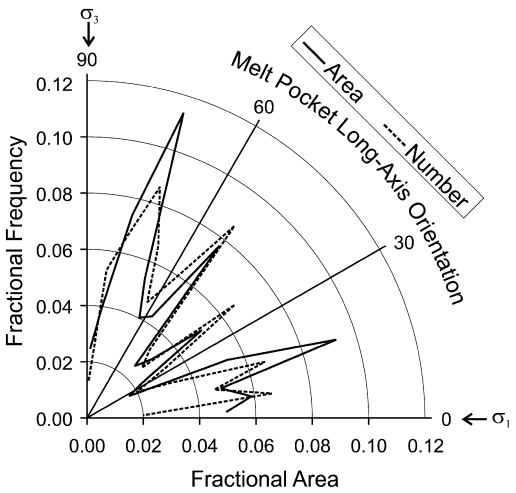

Fig. 6. Polar plot showing melt pocket long-axis orientations relative to the principal stresses for sample SA11 (low-stress deformation without microcracking). A total of 151 melt pockets in the BSE image were traced by hand. There is no significant melt-pocket preferred orientation.

The large grain size of the quartz coupled with the high viscosity of the melt is probably responsible for the fact that in all samples tested there is no overall textural equilibration of grain shape with the melt phase. Only small quartz fragments (ca. 10 μm diameter) show textural equilibration with the melt (i.e. subhedral to euhedral grain shapes) and there is some evidence of local formation of equilibrium dihedral angles at solid–solid–melt interfaces. For this reason, and also on account of the large melt fractions used, it was considered pointless to attempt to measure dihedral angles to evaluate the connectivity of the melt as was done by Cooper and Kohlstedt (1984) and Jurewicz and Watson (1984). Grain boundaries from which all melt appears to be displaced are very rare and the matrix of solid grains appears to be supported almost entirely at point contacts.

Relatively low magnification optical micrographs were used for grain size and shape analysis. Grain boundaries on these images are traced by hand and then the tracing was scanned. From the scanned image the area and long-axis orientation of each grain was calculated. From the area the diameter of a circle with the same area was used as an approximation of the grain size. A grain size distribution for sample SA20 (undeformed) is shown in Fig. 7a, and for sample SA12 (deformed at high differential stresses) in Fig. 7b. Fig. 8 is a polar histogram of grain long axis orientation for sample SA20. There is a weak preferred orientation of the grain long axes to be parallel to the maximum extension direction in this sample, but not in samples deformed only to lower differential stresses.

There is some evidence, in the form of wavy extinction associated with grain impingements, of intracrystalline plastic distortion (Fig. 5). Some optical strain features may have been inherited from the parent grains. The boundaries of the quartz grains are commonly serrated,

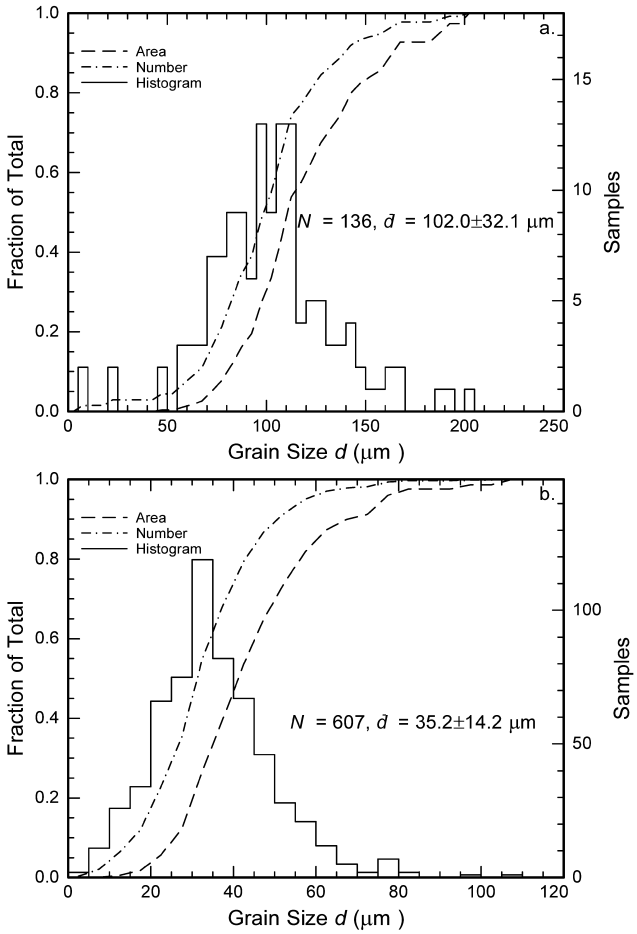

Fig. 7. Cumulative (fractional number of grains and fractional area of grains) and normal histograms showing the planar grain size distribution (no stereological correction) for (a) sample SA20 (undeformed) and (b) sample SA12 (high-stress deformation). The grain size reported is the diameter of a circle with the same area. For SA20 (a) a total of 136 grains were traced from micrographs and the mean grain size is 102 ± 32 μm. For SA12 (b) a total of 607 grains were traced from micrographs and the mean grain size is 35 ± 14 μm.

giving the appearance that the grains are being eroded, or alternatively overgrown. Most samples also show many small (ca. 10 μm) rounded to subhedral grains (Fig. 4). These grains could have been formed by (i) differences in the rate of melting along the grain boundary resulting in the formation of a serrated grain boundary and with further melting of the grains the formation of small quartz grains floating in the melt. (ii) crystallization from the melt, where it becomes is supersaturated in silica, or (iii) diffusive rounding of small fragments spalled from the parent grains during hot-pressing or deformation. Such small, rounded grains were best developed in wet samples. Some quartz may have crystallized as overgrowths on the host grains giving a serrated appearance to the grains. The lack of any observable shape change of the grains and the relatively small amount of optical strain features and microcracking of the grains (except in samples deformed to the highest differential stresses) relative to the strains imposed implies

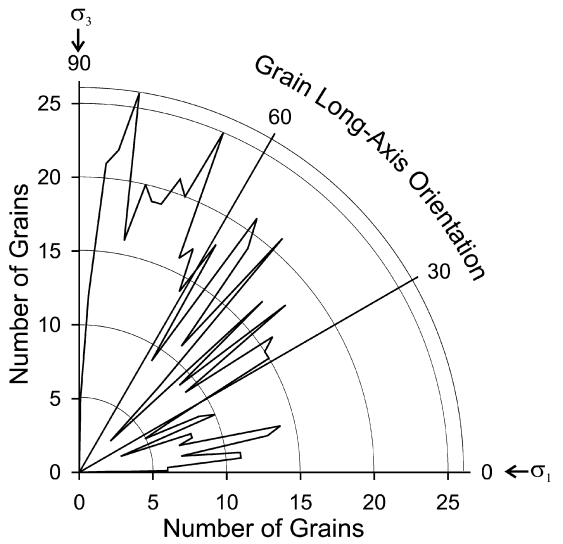

Fig. 8. Polar plot of grain long-axis orientation relative to the principal stress directions for sample SA12 (high-stress deformation with some axial microcracking), obtained using tracings of a total of 607 grains from micrographs. There is a clear elongation of grains parallel to the least principal stress.

that relative movement of the grains accommodated the majority of the sample deformation.

6. Discussion

Rutter (1997) and Paterson (2001) proposed simple models for diffusion-accommodated granular flow of partially molten rocks, both based on an earlier model of Paterson (1995) for granular flow facilitated by intergranular water. Under undrained conditions (volumetric strain rate = 0) for axisymmetric shortening deformation these predict approximately for the distortional strain rate, $\dot{\epsilon}$:

$$\dot{\epsilon} = \frac{CVD\phi^m}{d^2 \mathrm{R}T}(\sigma_1 - \sigma_3) \tag{2}$$

in which ϕ is the volume fraction of melt and m is taken to be two. V is the molar volume of the solid phase, D is the diffusivity of silica in the melt phase and d is the grain diameter. R is the universal gas constant and T is temperature in Kelvin. C is given by:

$$C = \frac{3\sqrt{\pi}}{2}\left(1 - 0.4\phi^{\frac{2}{3}}\right)^{\frac{-3}{2}} \tag{3}$$

This function describes strain-rate enhancement due to the effect of the presence of a melt phase on the applied stress and the diffusion pathway and is ~3 when $\phi = 0.2$. The main temperature sensitivity is contained within the Arrhenius term in D. D ($m^2\ s^{-1}$) is also related to the melt viscosity η (Pa s) through the empirical relation of Chekhmir and Epel'baum (1991):

$$\log_{10} D = -10.633 - 0.58\log_{10}\eta \tag{4}$$

The activation enthalpy, H, for silica diffusion can be approximated from the data of Persikov et al. (1990) using:

$$H(\text{kJ mol}^{-1}) = -10^{2.38}\psi^{-0.155} \quad (5)$$

in which ψ is the melt water content (wt%). Volume change during deformation related to changes in grain packing are neglected, although in practice these will cause fluctuations in melt pressure and hence in effective confining pressure.

We compare the predictions of Eq. (2) with the experimental data in Fig. 3 for similar conditions. Whilst bearing in mind the uncertainties inherent in the theoretical model, it predicts that slower strain rates than accessed in the laboratory experiments would be required to bring about deformation dominated by a diffusion controlled granular flow process (Fig. 3). Furthermore, a transition to a linear viscous rheology at lower strain rates means that partially molten granitic rocks will be extremely weak in nature. Eq. (2) predicts a flow strength for a partially molten granite of less than 1 MPa at a strain rate of $10^{-13}\,\text{s}^{-1}$ and a temperature of 800 °C with a melt fraction of 0.23 (defined by the temperature and protolith water content, here chosen to be 1 wt%, using Clemens and Vielzeuf (1987). The melt viscosity was estimated after Hess and Dingwell (1996) assuming all the water is in the melt phase and the diffusivity of the melt was calculated from this viscosity using Eq. (4) (Chekhmir and Epel'baum, 1991). The most promising route to access linear-viscous flow in the laboratory seems to be to plan experiments at smaller grain sizes whilst adding water to the melt to help reduce viscosity and enhance diffusivity. In this way Dell'Angelo et al. (1987) and Dell'Angelo and Tullis (1988) succeeded in producing a switch from dislocation creep at large grain sizes to diffusion creep at low grain sizes in partially molten aplites at 1500 MPa confining pressure.

The experimental data show that almost doubling the melt fraction (from ca. 16 to 28%) produces an acceleration of deformation rate by about 160 times at the same stress level and temperature (Fig. 3). The diffusion-accommodated granular flow model predicts approximately a five times increase in deformation rate for the same change in melt fraction. It is instructive to estimate the likely acceleration in strain rate to that expected for a further doubling of melt fraction. Behaviour at 60% melt fraction is likely to be dominated by the viscous flow of the melt. The melt viscosity is about 10^7 Pa s under anhydrous conditions (estimated following Holtz et al., 1999). At 10 MPa flow stress this corresponds to a strain rate of about $3 \times 10^{-1}\,\text{s}^{-1}$, or about 10^6 faster at 10 MPa flow stress than the sample with 28% melt. Thus there appears to be an accelerating trend of strain rate enhancement with increasing melt fraction. These figures also help to emphasise the sensitivity of strength and deformation rate to small variations in melt fraction, and suggest that the observed scatter in strain rate observed in the nominally 16% melt fraction samples is likely to be attributable to variations in melt fraction between samples that are difficult to control.

Because only two different melt fractions are reported here it is difficult to shed any more light on the existence or not of a rheologically critical melt percentage (RCMP). However, it should be pointed out when considering this that in nature the first melts evolved from fluid-absent incongruent melting reactions will have a lower viscosity than the melts that evolve at higher degrees of melting (see Clemens and Vielzeuf, 1987; Holtz and Johannes, 1994). This is due firstly to the water content of the melt falling with increasing degree of melting, and secondly due to the associated progressive increase in more refractory elements in the melt. Hence through the progressive evolution of melt composition the effective value of the RCMP may not correspond simply to that deduced from experimental studies at constant melt composition.

Hirth and Kohlstedt (1995a,b) were able to demonstrate in olivine aggregates pervaded by basaltic melt the transition from flow dominated by dislocation creep of the solid phase to diffusion creep accelerated by the intergranular melt. For this system it is possible to bring about intracrystalline flow readily in olivine aggregates in a gas medium apparatus. Also the low viscosity of the basaltic melt allows much finer grain sizes and lower melt fractions to be used without encountering problems related to melt pressure fluctuations.

Apart from the observed lack of evidence for significant intracrystalline plasticity throughout the quartz grains in this study, such a flow mechanism would not be expected to be important in experiments such as these. Attempts to produce intracrystalline plastic flow in quartz or quartzites in gas medium apparatus at 300 MPa confining pressure have generally not been successful except where the quartz has a high structure-bound water content (Hobbs et al., 1972; Luan and Paterson, 1992; Brodie and Rutter, 2000). Thus intracrystalline plastic flow is seen in wet, synthetic quartz (Hobbs et al., 1972; Luan and Paterson, 1992), or in quartz aggregates coarsened under pressure in a wet atmosphere (Luan and Paterson, 1992; Brodie and Rutter, 2000). If, in nature, partially molten granitic rocks follow a diffusion-accommodated granular flow process described by Eq. (2), then extrapolation to geological strain rates of the most recent flow law data (see Brodie and Rutter, 2000) for the intracrystalline plastic flow of even wet quartz will always result in higher flow stresses than required for flow of the partially molten granite, except at low temperatures (see Rutter, 1997, fig. 4.5, p. 89). Unequivocal evidence for intracrystalline plastic flow being active under supersolidus conditions in naturally deformed granitic rocks is rare (but see Miller and Paterson, 1994; Tribe and D'Lemos, 1996; Rosenberg and Riller, 2000). On the other hand, in synkinematic granites, supersolidus granular flow is common, tending to overprint evidence for any supersolidus intracrystalline plastic or granular flow.

A number of experimental investigations into the

rheology of partially molten granitic rocks, including this study, have found stress exponents ($d\log\dot{\epsilon}/d\log\sigma$) significantly greater than unity (e.g. van der Molen and Paterson, 1979; Rutter and Neumann, 1995). This suggests that a diffusive mass transfer process is not rate-controlling. In tests performed at the high end of the range of differential stresses encountered in this study, there was clear evidence that transgranular, axially oriented microcracking contributed significantly to the deformation (Fig. 5), and this would be expected to lead to a non-linear flow stress versus strain rate relationship. On the other hand, the microstructures observed in tests at low differential stresses suggest some kind of granular flow between the solid particles without evident microcracking. The usual explanation advanced for stress exponents greater than unity, in solid-state flow, is that the sample is deforming by intracrystalline plasticity where the strain is being accommodated by the movement of dislocations within the grains that make up the polycrystalline aggregate. For reasons given above this process has been discounted as dominant. A possible process that might explain the non-linearity involves sintering of the solid framework grains at their points of contact by neck growth. From time to time the contact points must rupture to permit sliding events between grains. At sufficiently slow strain rates this unsticking can be achieved by local diffusive transfer of silica (compare the serrated grain boundary sliding process of Raj and Ashby (1971)). At higher deformation rates this might be achieved by shear or extensional crack growth at the contact points, with the kinetics enhanced by the corrosive action of the intergranular melt phase. The limited intracrystalline plasticity observed at the grain contacts would also produce the same effect, and may occur in combination with a brittle process. Owing to the stress concentration that occurs at a crack tip relative to the remotely applied stresses, such processes are expected to be characterized by a non-linear stress/strain rate relationship (e.g. Atkinson and Meredith, 1981), and qualitatively might account for the non-linear flow observed in this study. It is difficult to assess the applicability of such a mechanism to natural deformation of partially molten granite because as yet very little is known about the conditions under which it is favoured. However, it is probably important to point out that slow natural deformations will tend to favour deformation mechanisms with a linear-viscous rheology. The lower stress exponents seen in experiments with water added, is most likely due to an increased component of sample deformation occurring by diffusive mass transfer processes, facilitated by the lower melt viscosity in these experiments.

7. Conclusions

At laboratory strain rates between 10^{-5} and 10^{-8} s^{-1} a synthetic, partially molten 'granitic' rock with a high viscosity melt phase deformed in a fully ductile manner by a mechanism that yields a non-Newtonian rheology. The absence of any evidence for strain being accommodated by change in shape of the grains and the lack of optical strain features within the quartz grains except at point contacts indicates that the quartz grains did not deform significantly by intracrystalline plasticity. Also, the flow stresses observed were too low to deform dry, natural quartz plastically at these strain rates other than transiently. At the highest stresses attained (at strain rates between 10^{-5} and 10^{-4} s^{-1}) there was evidence for significant strain involving oriented microcracking of grains.

At lower (including natural) strain rates it is expected on theoretical grounds that linear-viscous deformation mechanisms will become competitive, and cause an even greater divergence between the strength of the partially molten rock and the stress levels required to activate intracrystalline flow. In order to be able to extrapolate experimental data for partially molten granitic rocks to nature it must be established at what strain rates, melt viscosities, melt fractions and grain sizes the deformation of these rocks changes from a non-linear to a linear rheology (as inferred by Dell'Angelo et al., 1987). The results reported here will aid in the design of such experiments.

Acknowledgements

JM acknowledges receipt of a NERC postgraduate research studentship. This work was supported by UK NERC grants GR9/2640 and GR3/13062. The authors would like to acknowledge Lisa Dell'Angelo and Claudio Rosenberg for their constructive reviews. Experimental work was aided by experimental officer Robert Holloway.

References

Arzi, A.A., 1978. Critical phenomena in the rheology of partially melted rocks. Tectonophysics 44 (1–4), 173–184.

Atkinson, B.K., Meredith, P.G., 1981. Stress corrosion cracking of quartz: a note on the influence of chemical environment. Tectonophysics 77, 1–11.

Brodie, K.H., Rutter, E.H., 2000. Deformation mechanisms and rheology: why marble is weaker than quartzite. Journal of the Geological Society 157, 1093–1096.

Chekhmir, A.S., Epel'baum, M.B., 1991. Diffusion in magmatic melts; new study. In: Perchuk, L.L., Kushiro, I. (Eds.), Physical Chemistry of Magmas, Advances in Physical Geochemistry 9, Springer, New York, NY, pp. 99–119.

Clemens, J.D., Vielzeuf, D., 1987. Constraints on melting and magma production in the crust. Earth and Planetary Science Letters 86 (2), 287–306.

Cooper, R.F., Kohlstedt, D.L., 1984. Solution–precipitation enhanced diffusional creep of partially molten olivine–basalt aggregates during hot-pressing. Tectonophysics 107 (3–4), 207–233.

Covey-Crump, S.J., 1992. Application of a state variable description of inelastic deformation to geological materials. Unpublished Ph.D. thesis, University College London.

Dell'Angelo, L.N., Tullis, J., 1988. Experimental deformation of partially

melted granitic aggregates. In: Tracy, R.J., Day, H.W. (Eds.), Studies in the Genesis and Deformation of Migmatites, Journal of Metamorphic Geology 6, Blackwell, Oxford, pp. 495–515.

Dell'Angelo, L.N., Tullis, J., Yund, R.A., 1987. Transition from dislocation creep to melt-enhanced diffusion creep in fine-grained granitic aggregates. Tectonophysics 139 (3–4), 325–332.

Fischer, G.J., Paterson, M.S., 1989. Dilatancy during rock deformation at high temperatures and pressures. Journal of Geophysical Research, B, Solid Earth and Planets 94 (12), 17,607–17,617.

Gleason, G.C., Tullis, J., 1995. A flow law for dislocation creep of quartz aggregates determined with the molten salt cell. Tectonophysics 247, 1–23.

Gleason, G.C., Bruce, V., Green, H.W., 1999. Experimental investigation of melt topology in partially molten quartzo-feldspathic aggregates under hydrostatic and non-hydrostatic stress. Journal of Metamorphic Geology 17 (6), 705–722.

Hess, K.-U., Dingwell, D.B., 1996. Viscosities of hydrous leucogranitic melts: a non-Arrhenian model. American Mineralogist 81, 1297–1300.

Hirth, G., Kohlstedt, D.L., 1995a. Experimental constraints on the dynamics of the partially molten upper mantle; deformation in the diffusion creep regime. Journal of Geophysical Research 100 (B2), 1981–2001.

Hirth, G., Kohlstedt, D.L., 1995b. Experimental constraints on the dynamics of the partially molten upper-mantle. 2. Deformation in the dislocation creep regime. Journal of Geophysical Research 100 (B8), 15441–15449.

Hobbs, B.E., McLaren, A.C., Paterson, M.S., 1972. Plasticity of single crystals of synthetic quartz. In: Heard, H.C., Borg, I.Y., Carter, N.L., Raleigh, C.B. (Eds.), Flow and Fracture of Rocks, Geophysical Monographs 16, American Geophysical Union, Washington, DC, pp. 29–53.

Holtz, F., Johannes, W., 1994. Maximum and minimum water contents for granitic melts: implications for chemical and physical properties of ascending magmas. Lithos 32, 149–159.

Holtz, F., Roux, J., Ohlhorst, S., Beherens, H., Schulze, F., 1999. The effects of silica and water on the viscosity of hydrous quartzo-feldspathic melts. American Mineralogist 84, 27–36.

Jurewicz, S.R., Watson, E.B., 1984. Distribution of partial melt in a felsic system—the importance of surface-energy. Contributions to Mineralogy and Petrology 85 (1), 25–29.

Kirschen, M., Pichavant, M., 2001. A thermodynamic model for hydrous silicate melts in the system $NaAlSi_3O_8$–$KAlSi_3O_8$–Si_4O_8–H_2O. Chemical Geology 174 (1-3), 103–114.

Luan, F.C., Paterson, M.S., 1992. Preparation and deformation of synthetic aggregates of quartz. Journal of Geophysical Research 97 (B1), 301–320.

Miller, R.B., Paterson, S.R., 1994. The transition from magmatic to high-temperature solid-state deformation—implications from the Mount Stuart Batholith, Washington. Journal of Structural Geology 16 (6), 853–865.

van der Molen, I., Paterson, M.S., 1979. Experimental deformation of partially-melted granite. Contributions to Mineralogy and Petrology 70 (3), 299–318.

Nelson, K.D., Zhao, W., Brown, L.D., Kuo, J., Che, J., Liu, X., Klemperer, S.L., Makovsky, Y., Meissner, R., Mechie, J., Kind, R., Wenzel, F., Ni, J., Nabelek, J., Chen, L., Tan, H., Wei, W., Jones, A.G., Booker, J., Unsworth, M., Kidd, W.S.F., Hauck, M., Alsdorf, D., Ross, A., Cogan, M., Wu, C., Sandvol, E.A., Edwards, M., 1996. Partially molten middle crust beneath southern Tibet; synthesis of Project INDEPTH results. Science 274 (5293), 1684–1688.

Paquet, J., Francois, P., 1980. Experimental deformation of partially melted granitic rocks at 600–900 °C and 250 MPa confining pressure. Tectonophysics 68 (1–2), 131–146.

Paquet, J., Francois, P., Nedelec, A., 1981. Effect of partial melting on rock deformation; experimental and natural evidences on rocks of granitic compositions. Tectonophysics 78 (1–4), 545–565.

Paterson, M.S., 1990. Rock deformation experimentation. In: Duba, A.G., Durham, W.B., Handin, J.W., Wang, H.F. (Eds.), The Brittle–Ductile Transition in Rocks, Geophysical Monograph 56, American Geophysical Union, Washington, DC, pp. 187–194.

Paterson, M.S., 1995. A theory for granular flow accommodated by material transfer via an intergranular fluid. Tectonophysics 245 (3–4), 135–151.

Paterson, M.S., 2001. A granular flow theory for the deformation of partially molten rock. Tectonophysics 335 (1–2), 51–61.

Persikov, E.S., Zharikov, V.A., Bukhtiyarov, P.G., Polskoy, S.F., 1990. The effect of volatiles on the properties of magmatic melts. European Journal of Mineralogy 2 (5), 621–642.

Raj, R., Ashby, M.F., 1971. grain boundary sliding and diffusional creep. Metallurgical Transactions 2 (4), 1113–1127.

Renner, J., Evans, B., Hirth, G., 2000. On the rheological critical melt percentage. Earth and Planetary Science Letters 181, 585–594.

Rosenberg, C.L., Riller, U., 2000. Partial-melt topology in statically and dynamically recrystallized granite. Geology 28 (1), 7–10.

Rutter, E.H., 1997. The influence of deformation on the extraction of crustal melts: a consideration of the role of melt-assisted granular flow. In: Holness, M.B., (Ed.), Deformation-enhanced Fluid Transport in the Earth's Crust and Mantle, The Mineralogical Society Series 8, Chapman & Hall, London, pp. 82–110.

Rutter, E.H., Neumann, D.H.K., 1995. Experimental deformation of partially molten Westerly Granite under fluid-absent conditions, with implications for the extraction of granitic magmas. Journal of Geophysical Research 100 (B8), 15,697–15,715.

Rutter, E.H., Atkinson, B.K., Mainprice, D.H., 1978. On the use of the stress relaxation testing method in the studies of the mechanical behaviour of geological materials. Geophysical Journal of the Royal Astronomical Society 55 (1), 155–170.

Sawyer, E.W., 2001. Melt segregation in the continental crust: distribution and movement of melt in anatectic rocks. Journal of Metamorphic Geology 19 (3), 291–309.

Tribe, I.R., D'Lemos, R.S., 1996. Significance of a hiatus in down-temperature fabric development within syn-tectonic quartz diorite complexes, Channel Islands, UK. Journal of the Geological Society 153, 127–138.

Viskupic, K.M., Renner, J., Hirth, G., Evans, B., 2001. Melt segregation from partially molten peridotites. EOS, AGU Transactions 82, F1107–F1108.

Wen, S., Nekvasil, H., 1994. Ideal associated solutions; application to the system albite–quartz–H_2O. American Mineralogist 79 (3–4), 316–331.